

Shaking table tests on seismic response of backdrop metal ceilings

Tie G. Zhou*¹, Shuai S. Wei^{1a}, Xiang Zhao¹, Le W. Ma², Yi M. Yuan¹ and Zheng Luo¹

¹ School of Civil Engineering, Xi'an University of Architecture & Technology, Shaanxi, China

² Key Lab of Structure Engineering and Earthquake Resistance, Ministry of Education (XAUAT), China

(Received May 16, 2019, Revised August 23, 2019, Accepted September 5, 2019)

Abstract. In recent earthquakes, the failure of ceiling systems has been one of the most widely reported damage and the major cause of functionality interruption in some buildings. In an effort to mitigate this damage, some scholars have studied a series of ceiling systems including plaster ceilings and mineral wool ceilings. But few studies have involved the backdrop metal ceiling used in some important constructions with higher rigidity and frequency such as the main control area of nuclear power plants. Therefore, in order to evaluate its seismic performance, a full-scale backdrop metal ceiling system, including steel runners and metal panels, was designed, fabricated and installed in a steel frame in this study. And the backdrop metal ceiling system with two perimeter attachments variants was tested: (i) the ends of the runners were connected with the angle steel to form an effective lateral constraint around the backdrop metal ceiling, (ii) the perimeter attachments of the main runner were retained, but the perimeter attachments of the cross runner were removed. In the experiments, different damage of the backdrop metal ceiling system was observed in detail under various earthquakes. Results showed that the backdrop metal ceiling had good integrity and excellent seismic performance. And the perimeter attachments of the cross runner had an adverse effect on the seismic performance of the backdrop metal ceiling under earthquakes. Meanwhile, a series of seismic construction measures and several suggestions that need to be paid attention were proposed in the text so that the backdrop metal ceiling can be better applied in the main control area of nuclear power plants and other important engineering projects.

Keywords: nuclear power plant; backdrop metal ceiling system; shaking table test; seismic design; seismic performance

1. Introduction

A backdrop ceiling is a suspended ceiling with two level planes, which similar to a stepped form and a staggered floor in the building, as shown in Fig. 1.

Backdrop metal ceiling systems have often been widely used in some important buildings such as the main control area of nuclear power plants. The backdrop metal ceiling (BMC) has the advantages of beautiful appearance and convenient ventilation system maintenance. And it also can effectively utilize the space when the ventilation ducts are arranged above low plane.

In recent earthquakes, the failure of BMC and other ceiling systems has been one of the most widely reported damage in buildings (Badillo-Almaraz *et al.* 2006, Gilani *et al.* 2010) and has often been reported as the major cause of functionality interruption and, in some cases, may endanger the safety of people (Echevarria *et al.* 2012, Soroushian *et al.* 2016a). The damage of ceiling systems in some important buildings such as stadium, nuclear power plant, and hospital is shown in Fig. 2. In a stadium, the panels of ceiling system were derailed and even fell (see Fig. 2(a)). In a nuclear power plant, the failure of ceiling grid members was occurred (see Fig. 2(b)). And in a hospital, extensive



Fig. 1 The backdrop ceiling

damage of ceiling system was observed (see Fig. 2(c)). All these damage of ceiling systems may cause the functionality interruption of buildings and serious or even unpredictable consequences. Therefore, there is an urgent need to investigate the seismic performance of ceiling systems.

In the past 20 years, some scholars have studied a series of ceiling systems through the shaking table tests which were considered to be a reliable approach to assess the seismic performance of the ceilings (Lu *et al.* 2018). Yao (2000) studied the DHS ceiling system and revealed that use of the pop rivets at the molding can increase the seismic performance. Badillo-Almaraz (2004) carried out shaking table tests on the ceilings with different assembly forms, and gave the seismic fragility curves corresponding to different degrees of damage in the corresponding assembly form. Magliulo *et al.* (2012) studied the seismic behavior of plasterboard continuous suspended ceilings under strong earthquakes. Watakabe *et al.* (2012) studied the failure

*Corresponding author, Professor,
E-mail: zhoutiegang123@163.com
^aMaster, E-mail: wei1326421371@163.com



(a) 2008 Inland earthquake in Iwate Miyagi



(b) The 2011 earthquake of the Pacific coast of Tōhoku



(c) 2013 Lushan Ms 7.0 Earthquake

Fig. 2 Ceiling damage in earthquakes

mechanism of ceiling connectors in large space structures and developed a seismically engineered suspended ceiling system in order to improve the seismic performance of conventional ceilings. Wang *et al.* (2016) conducted a series of shake table tests. The test results showed that the suspended ceiling in the actual earthquake was more likely to be destroyed than test. Ozcelik *et al.* (2016) studied SCS and found that clip-in ceiling system performs better than lay-on system regardless of material and workmanship qualities. Lu *et al.* (2018) evaluated the seismic performance of suspended ceilings attached to large-span spatial structures and proposed a system with a hinge in the middle of the hanger rod to limit the transmission of vertical vibration.

However, few studies have involved the backdrop metal ceiling used in some important constructions with higher rigidity and frequency such as the main control area of nuclear power plants. If the ceilings of nuclear power plants fail, the ceilings may further cause damage to precision instruments, endanger the nuclear island and even cause unpredictable consequences. Therefore, the seismic performance of backdrop metal ceilings is also worthy of attention. In this paper, a steel frame and a full-scale BMC system, including hanger rods, steel runners, metal panels and lights, were designed, fabricated and installed for this purpose. In real structures behavior of BMC system in seismic conditions will depend on a many of parameters that will affect their amplification. One of the most important parameter is boundary conditions of the construction. Therefore, we referred to the treatment of the border by Radnić *et al.* (2015) and Banović *et al.* (2018),

and tested BMC system with two perimeter attachments variants: (i) the ends of the runners were connected with the angle steel to form an effective lateral constraint around BMC system. (ii) the perimeter attachments of the main runner were retained, but the perimeter attachments of the cross runner were removed. The purpose is to investigate the perimeter attachments of the cross runner in the seismic performance of BMC system. Finally, the seismic performance and integrity of BMC system were evaluated and main conclusions of this research are given.

2. Experimental study

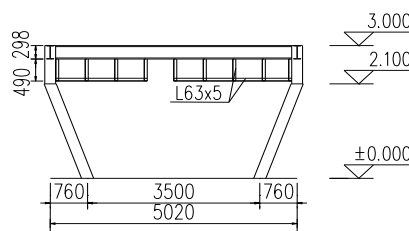
2.1 Test setup and specimens

The test was carried out at the Key Lab of Structure Engineering and Earthquake Resistance, Ministry of Education (XAUAT). With a payload capacity of 30 t, the shaking table is capable of generating peak x-direction motions of up to 1.2 g peak ground acceleration (PGA), producing peak y and z directions motions of up to 1.0 g PGA.

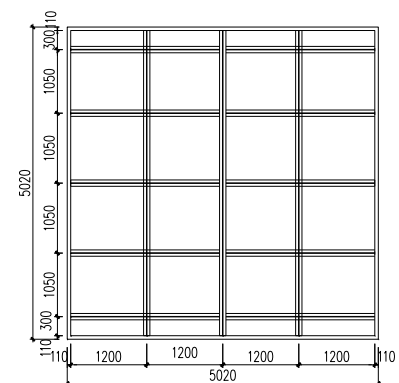
A steel frame of 5.0 m × 5.0 m (see Fig. 3) was designed, built and installed on the shaking table with purpose to simulate the seismic response of BMC system (see Figs. 4-5). Because the shaking table size limit (see Appendix I) cannot meet the ceiling installation size, the four steel columns were installed on the shaking table on a slant (see Fig. 3(a)). And the steel frame was connected to the shaking table with 16 M24 high-strength bolts. Then



(a) Test frame



(b) Elevation of steel frame



(c) Plan of steel frame

Fig. 3 Steel frame

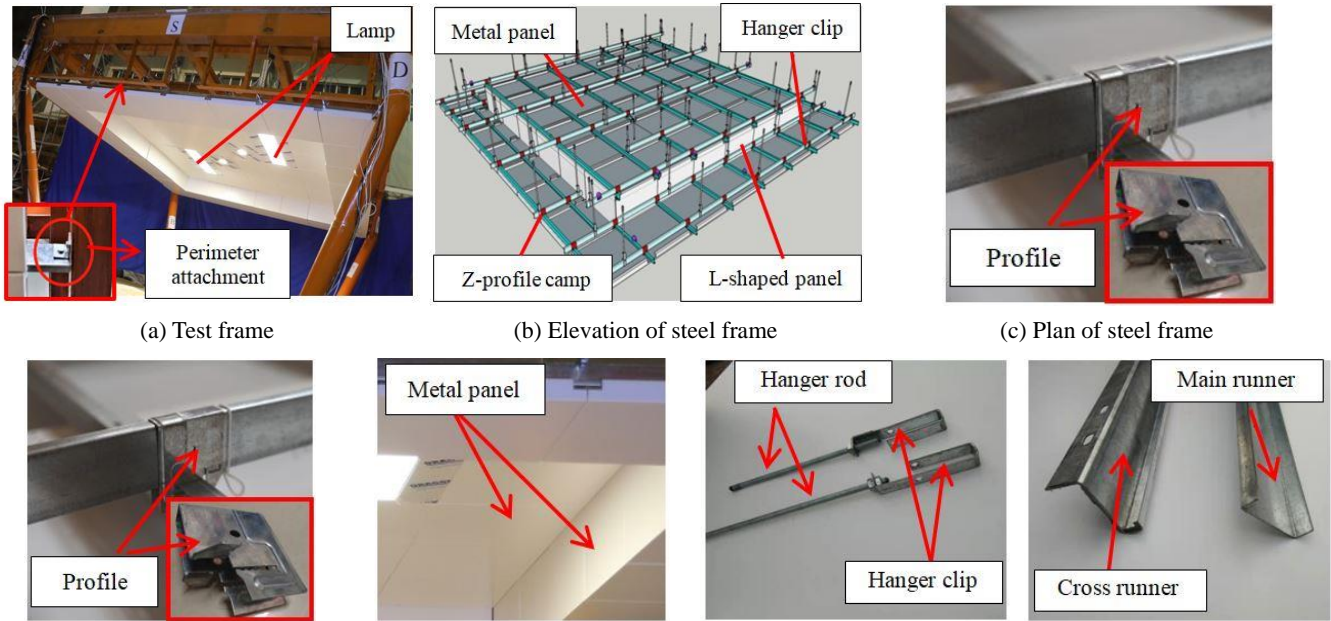


Fig. 4 Test specimen

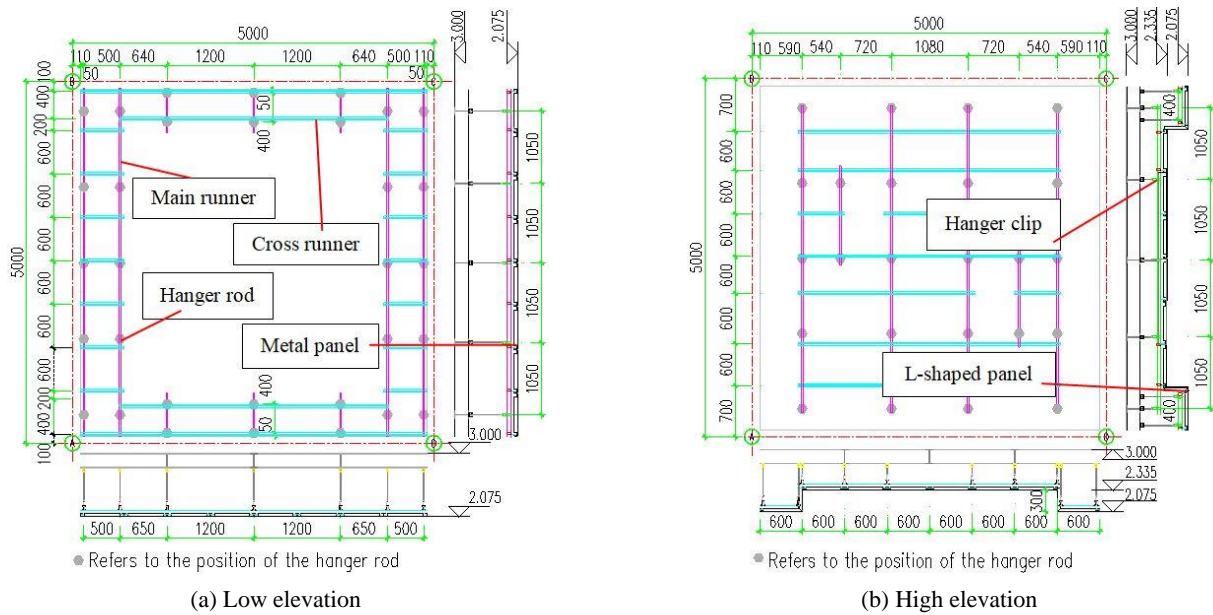


Fig. 5 Plan of BMC

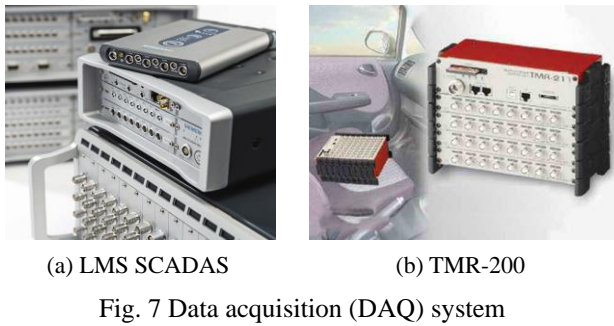
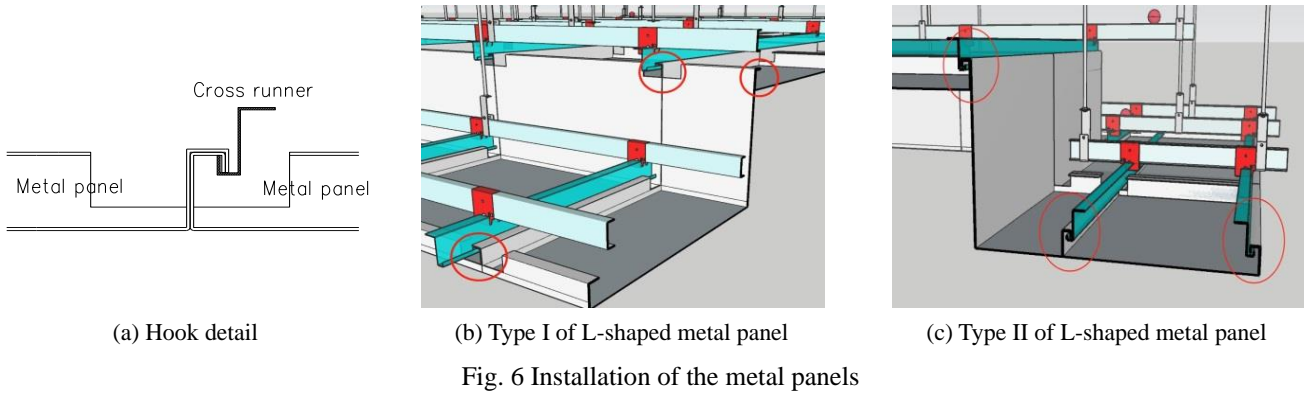
BMC system (0.3 t in weight) was suspended in the steel frame (3.3 t in weight).

The main structure of BMC system was designed and consisted of c-shape main runners, z-shape cross runners, metal panels and z-profile camp (see Fig. 4(b)), so that this structure can enhance the stability of the whole ceiling. Moreover, BMC was suspended by cross runner with z-profile camp (see Fig. 4). It can enhance the stability of BMC system. And the metal panels of BMC system were designed and hooked on the cross runners and hooked with other panel tightly (see Fig. 6(a)), instead of fixing the ceiling with self-tapping screws. At the backdrop, two types of L-shaped metal panels were selected and used for the anti-side force member to connect the two level planes,

which can more flexibly arrange the runners and facilitate construction. The L-shaped metal panels are shown in Figs. 6(b)-(c).

2.2 Instrumentation

In order to record the response of the steel frame and BMC system, accelerometers, displacement transducers, and strain gauges were arranged and installed in the steel frame, the hanger rods, the main runners, the cross runners, the joints and the metal panels. A LMS SCADAS (see Fig. 7(a)) was used to acquire the acceleration and displacement during the tests. And the strain was measured by a TMR-200 Dynamic Data Acquisition Instrument (see Fig. 7(b)).



The sampling rate during the tests was 50 Hz. In the tests, there are a total of 15 accelerometers, 12 displacement transducers, and 11 strain gauges. Table 1 and Fig. 8 show the measured point of the sensors. The measured point numbers are represented by I-II. Among I-II, I represents the sensor type, and II for measured position (II = 1, 2, ...). In addition, in order to check the real input transmitted to the steel frame and BMC system from the shaking table, one triaxial accelerometer was placed at the central of the shaking table.

Table 1 Instrument layout

Sensors	Number	Position	Sensors	Number	Position	Sensors	Number	Position
Accelerometers	1~4	Low runner	Displacement transducers	1~2	Angle steel	Strain gauges	1~4	Junction between the runner and the angle steel
	5~6	Low panel		3~4	Low panel		5~6	Hanger rod
	7~11	High runner		5~9	High runner		7	Z-profile camp
	12~14	High panel		10~12	Top of the steel frame		8~11	Upper flange of the runner

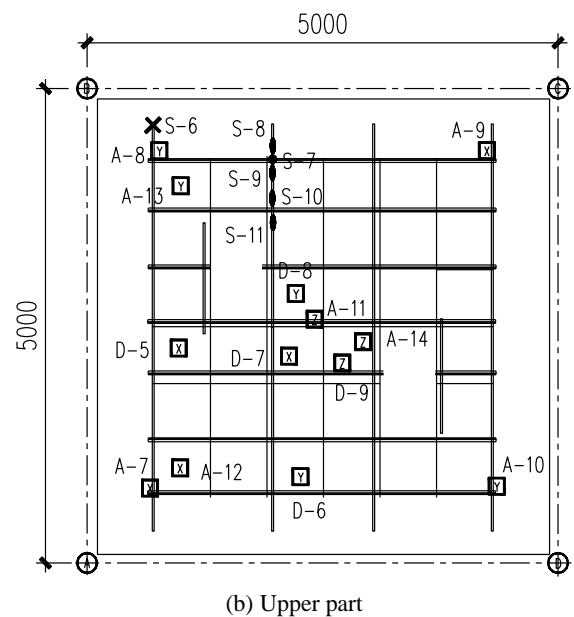
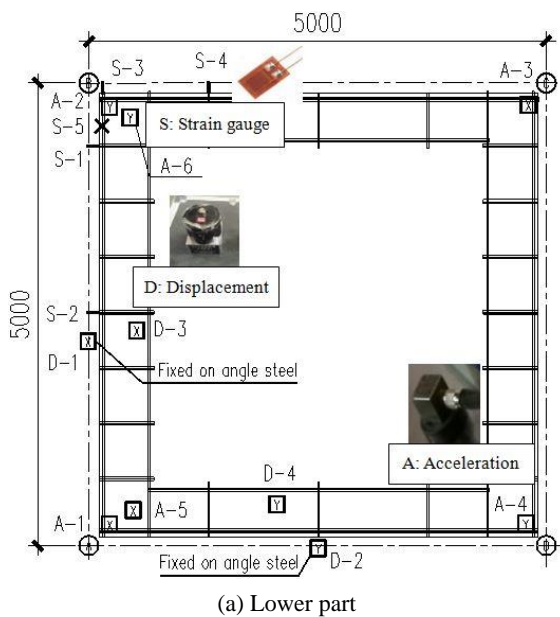


Fig. 8 Instrumentation of BMC

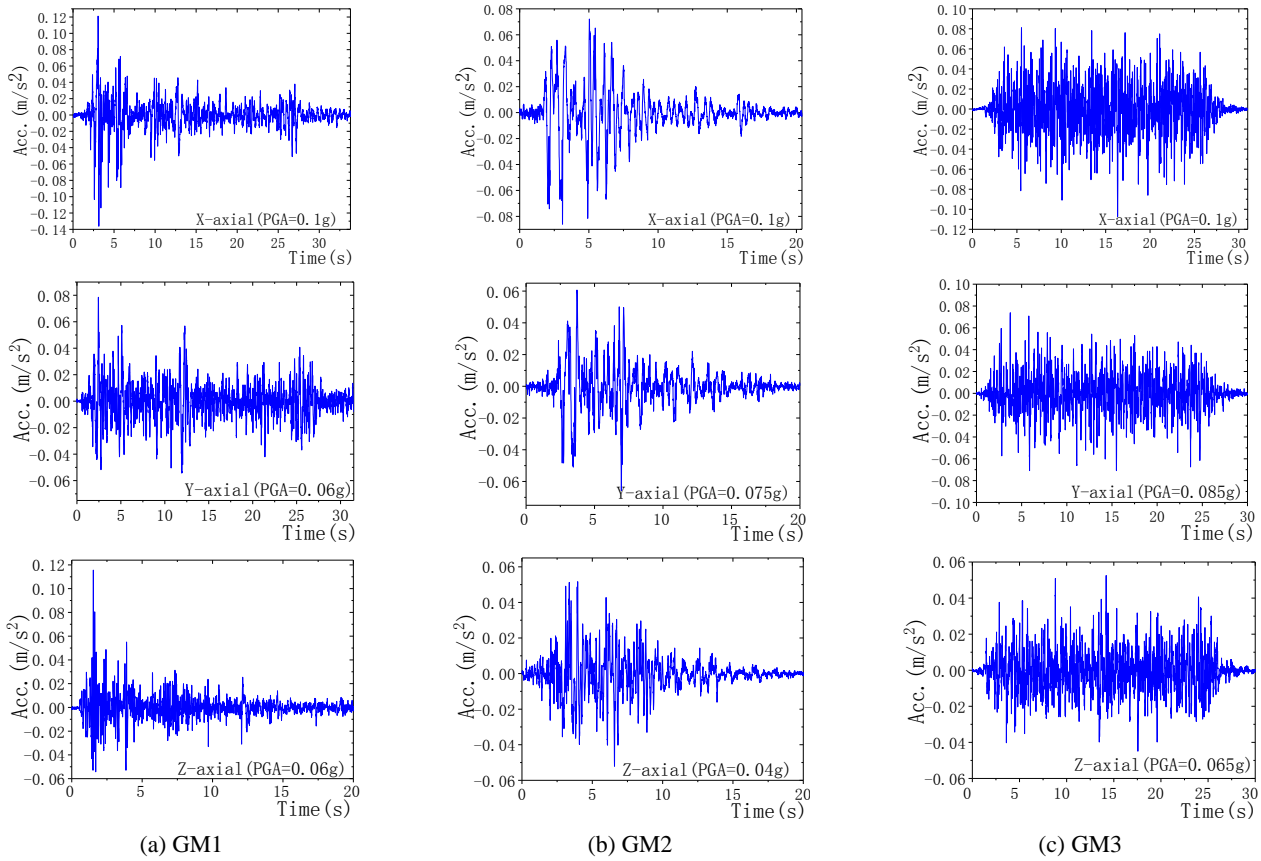


Fig. 9 Acceleration time history of ground motions

Table 2 Test protocol for shaking table test program

Case	Input motion	PGA(g)			Case	Input motion	PGA(g)			Case	Input motion	PGA(g)		
		X dir.	Y dir.	Z dir.			X dir.	Y dir.	Z dir.			X dir.	Y dir.	Z dir.
Phase I					III-8	Artificial	0.4	0.34	-	Phase IV				
I-1	White noise	0.05	0.05	0.05	III-9	Artificial	0.4	0.34	0.26	IV-1	White noise	0.05	0.05	0.05
I-2	Artificial	0.1	0.085	0.065	III-10	White noise	0.05	0.05	0.05	IV-2	El Centro	0.2	0.12	0.12
Phase II					III-11	El Centro	0.6	0.36	0.36	IV-3	Artificial	0.2	0.17	-
II-1	White noise	0.05	0.05	0.05	III-12	Kobe	0.6	0.45	0.24	IV-4	El Centro	0.4	0.24	0.24
II-2	Artificial	0.1	-	-	III-13	Artificial	0.6	0.51	-	IV-5	Artificial	0.4	0.34	-
II-3	Artificial	-	0.1	-	III-14	Artificial	0.6	0.51	0.39	IV-6	White noise	0.05	0.05	0.05
II-4	Artificial	-	-	0.1	III-15	White noise	0.05	0.05	0.05	IV-7	EL	0.6	0.36	0.36
Phase III					III-16	El Centro	0.8	0.48	0.48	IV-8	Artificial	0.6	0.51	-
III-1	White noise	0.05	0.05	0.05	III-17	Kobe	0.8	0.6	0.32	IV-9	White noise	0.05	0.05	0.05
III-2	El Centro	0.2	0.12	0.12	III-18	Artificial	0.8	0.68	-	IV-10	El Centro	0.8	0.48	0.48
III-3	Kobe	0.2	0.15	0.08	III-19	Artificial	0.8	0.68	0.52	IV-11	Artificial	0.8	0.68	-
III-4	Artificial	0.2	0.17	-	III-20	White noise	0.05	0.05	0.05	IV-12	White noise	0.05	0.05	0.05
III-5	Artificial	0.2	0.17	0.13	III-21	El Centro	1.0	0.6	0.6	IV-13	El Centro	1.0	0.6	0.6
III-6	El Centro	0.4	0.24	0.24	III-22	Artificial	1.0	0.85	-	IV-14	Artificial	1.2	0.85	-
III-7	Kobe	0.4	0.3	0.16	III-23	White noise	0.05	0.05	0.05	IV-15	White noise	0.05	0.05	0.05

2.3 Seismic inputs and testing protocol

The seismic inputs and protocols for shaking table tests always obey the rules that at least two sets of strong

earthquake records and one set of artificial acceleration time-history curves and should be selected based on the intensity, site class, and the design seismic group (Lu *et al.* 2018). According to the ground motion intensity, spectral

characteristics and duration of seismic waves (Bai and Jin 2007, Shen 2015), three ground motions were selected for this test series consisted of the 1940 El Centro ground motion (GM1), the Kobe ground motion (GM2) from the 1995 Kobe earthquake (Sato *et al.* 2011), and an artificial ground motion (GM3) according to Chinese seismic region of M8, site II. One of the reasons why GM1 and GM2 were selected for testing is that the site where the structure located is M8, site II ($T_g = 0.4$ s) according to the engineering background, which is close to the site type of GM1 and GM2 recorded by actual earthquake. Another reason is that the predominant period of GM1 and GM2 is consistent with the characteristic period of the site. The minimum duration of the three seismic waves is 30 s, which is greater than 10 times the structural fundamental period. And the time interval of the seismic waves is 0.02 s. In order to simulate the seismic response of BMC more realistically and effectively, the PGA ratio of GM1 and GM2 were adjusted according to the actual recording ratio, and the PGA ratio of GM3 was designed as $x:y:z = 1:0.85:0.65$ according to the requirements of GB50011-2010 (2016) and the most unfavorable situation. Fig. 9 shows the time histories of the three ground motions after time compression for scaling.

Table 2 lists the loading protocol of the shaking table test. The test was divided into four phases. In Phase I, without installation of the metal panels and the angle steel, white noise and GM3 was performed to test the channel of sensors. In Phase II, the metal panels were hooked on the steel runners, but the angle steels were not installed. The purpose is to obtain the vibration response of BMC without lateral restraint. In phase III, the angle steel was installed, and the ends of the runners were connected with the angle steel to form an effective lateral constraint. The seismic action gradually increased so that the response of BMC system under different PGA could be researched. In Phase IV, the perimeter attachments of the cross runner were removed, in order to study the influence of perimeter attachments of the cross runner on the seismic performance of BMC compare with phase III.

3. Experiments results and discussion

3.1 Self-vibration of specimens

Since the vibration input of BMC system is derived from the steel frame, the dynamic characteristics of the steel frame are critical to the response of BMC in earthquakes. The points measured the characteristics of the steel frame were mainly arranged at the top node of it. As an important structural component, a joint can transmit and allocate internal forces in the frame structural system, ensuring structural integrity and reflecting the dynamic characteristics of the entire steel frame (Zhang *et al.* 2018). Moreover, BMC was regarded as a single-degree-of-freedom (SDF) system in this paper, and only first-order self-vibration frequency (FSF) of BMC system was discussed. By the white noise excitation, the transfer function method (Han *et al.* 2014) can be used to obtain the FSF of the ceiling and the steel frame. The amplitude-

frequency figure of the acceleration response was obtained by the transfer function, and the frequency corresponding to the peak point on the amplitude-frequency figure is the FSF of specimen (Zhang 2002). In the transfer function, the acceleration at the top of the steel frame was taken as an input and the corresponding acceleration of BMC system was an output, and the FSF of BMC system can be obtained. Similarly, the acceleration at the shaking table top was used as input and the corresponding acceleration at the top of the steel frame was output, and the FSF of the steel frame can be obtained. Table 3 shows the FSF of the steel frame and BMC in partial phases. Fig. 10 shows the amplitude-frequency figure of BMC.

In the x-direction and y-direction, the FSF of the steel frame is between 8.98 Hz and 9.67 Hz. The FSF of BMC is basically at around 3 Hz, which is far lower than the FSF of the steel frame, indicating that BMC system has low rigidity when there is no lateral constraint around it. In the z-direction, the FSF of the steel frame is around 22 Hz, which is due to high stiffness of the steel frame. The behavior of steel frame significantly depends on frame stiffness (Baloevic *et al.* 2017). The steel frame designed in this manuscript has a high rigidity, good load-bearing capacity and can withstand large strains, which contributes a lot to the dynamic response of the pure ceiling (Baloevic *et al.* 2016). Also, we can conclude that the state of the steel frame always remained in the plastic limit during the experiments and the steel frame can be used as a good test platform for testing BMC system.

3.2 Observed damage

Table 4 lists the damage of BMC subjected to three ground motions. According to the damage phenomena, the main damage was found at the backdrop, including the metal panels derailed and fell (Figs. 11(d) and (h)), vertical vibration of the high panel (Fig. 11(e)), and the nuts loosened (Fig. 11(b)). The panels derailed and fell were mainly the beginning and end position of hook installation. That's because the constraints on these panels were weak, so the place where the failure occurred need to be pay

Table 3 FSF of specimens

Specimen	Test phase	Case	Directions		
			X	Y	Z
Steel frame	Phase I	I-1	8.98	8.5	22.66
	Phase II	II-1	9.28	9.18	22.46
	Phase III	III-1	9.67	9.57	22.46
		III-23	9.28	8.59	22.46
	Phase IV	IV-1	9.08	9.18	21.48
		IV-15	8.98	8.5	22.66
BMC system	Phase I	I-1	2.54	3.03	-
	Phase II	II-1	2.73	3.32	-

*Note: In phase III and phase IV, BMC system was connected with the steel frame, and there were boundary constraints around the ceiling. At this time, the FSF of BMC cannot be obtained

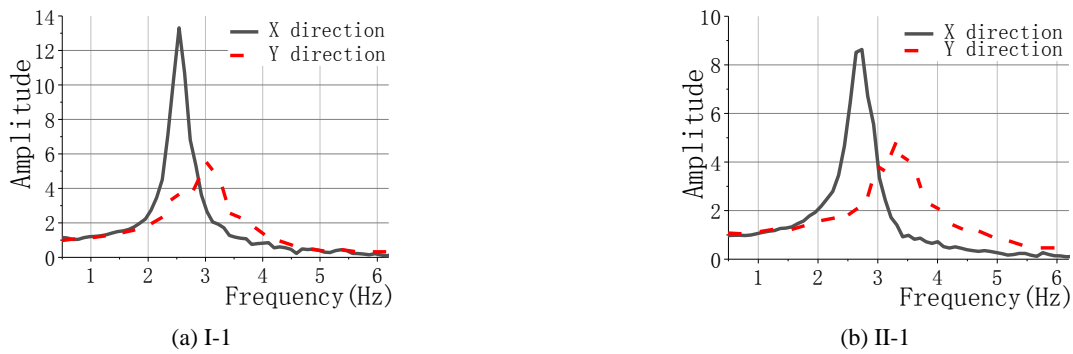


Fig. 10 Amplitude-frequency curves of BMC by white noise

Table 4 Damage observed during experiments

Test Phase	PGA (g)	Damage phenomena
Phase I	0.1	No damage
Phase II	0.1	No damage
Phase III	0.2	No damage
	0.4	Metal panels collided and produced sound; panels slightly slipped at the backdrop (AD side), about 1 cm
	0.6	BMC collided and produced a noise; two L-shaped metal panels derailed at the backdrop (Fig. 11(a)); nut loosened (Fig. 11(b))
	0.8	A loud collision sound; vertical vibration of metal panels, two metal panels derailed, one metal panel fell at the backdrop (AD side) (Fig. 11(c))
	1.0	Four metal panels derailed (Fig. 11(d)), vertical vibration of three high panels at the backdrop (AD side) (Fig. 11(e)); high cross runner slipped relative to panel (Fig. 11(f))
Phase IV	0.2	No damage
	0.4	Panels slipped at the backdrop (AD side), about 1.5 cm
	0.6	Slippage increased, about 2.5 cm; a loud noise
	0.8	Four metal panels derailed and one metal panel fell at the backdrop (AD side) (Fig. 11(g)); two high panels vibrated vertically; two high cross runners slipped relative to panel
	1.2	A loud collision sound; three metal panels derailed and two panels fell at the backdrop (AD side), and the metal panels derailed seriously at the backdrop (BC side) (Fig. 11(h))

*Note: During the test, BMC system would be repaired simply before the next case began

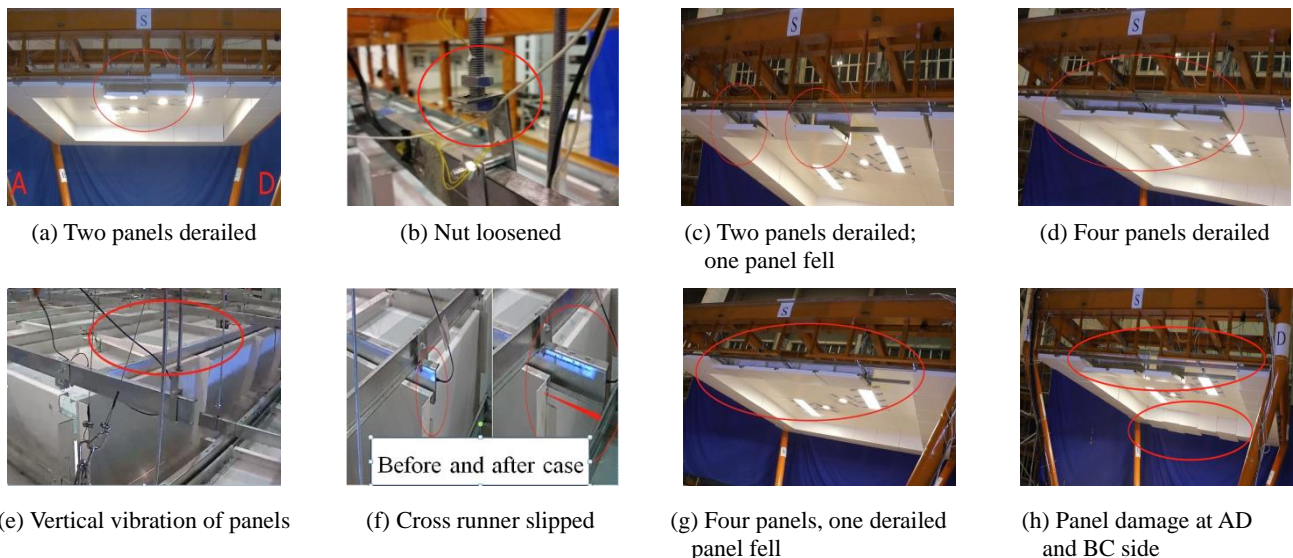


Fig. 11 Observed damage

attention. Besides above damage, relative slip was occurred between the metal panel and the runner due to the collision of BMC system under earthquakes (Fig. 11(f)). It is obvious that the friction between the z-profile camp and the cross runner was not enough to resist the external force. On the other hand, when $PGA = 0.6\text{ g}$, the damage of BMC system in phase III was more serious than the damage in the phase IV, but when $PGA \geq 0.8\text{ g}$, the damage of BMC system in phase IV was more serious than the damage in phase III. Despite the above damage, BMC system still remained intact during all experiments. After simple maintenance, it could be restored to pre-test state.

For the derailment of the metal panel, the L-shape runners were recommended to design at the ceiling-perimeter.

For the fell of the metal panels, the security wire was

proposed to install on the panel to prevent falling, especially in the main control area of nuclear power plants. For the nut loosened, plastic gasket with good deformation ability was suggested to add. For the problem of sound caused by collision between panels under earthquakes, soft contact in addition to the edge banding was advised to set around the panel to achieve a certain buffering effect.

3.3 Acceleration amplification of specimens

Fig. 12 shows the ratio between the peak acceleration at the top of the steel frame and PGA, that is, the acceleration amplification in the x-direction, y-direction and z-direction, respectively. The acceleration time history curves of the top of the shaking table/steel frame, with the GM1 (1.0 g) input, are shown in Fig. 13. It can be seen that the peak of the

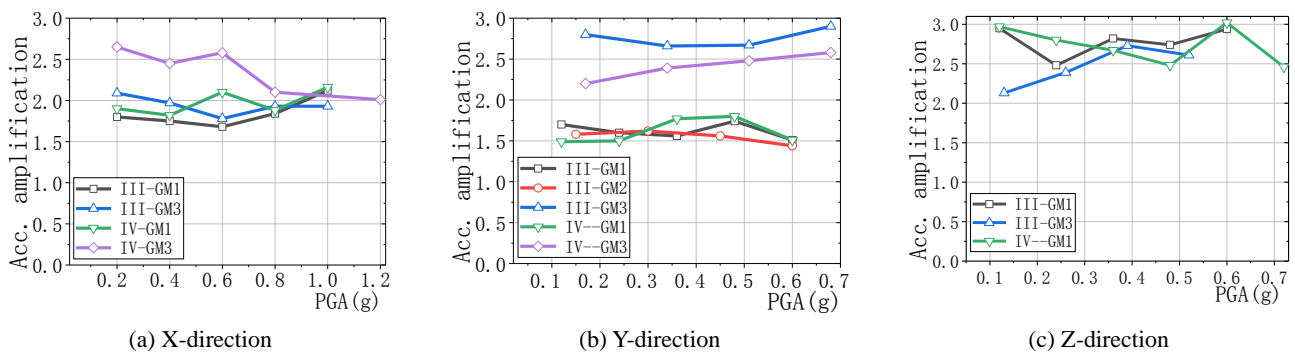


Fig. 12 Acceleration amplification at the top of the steel frame

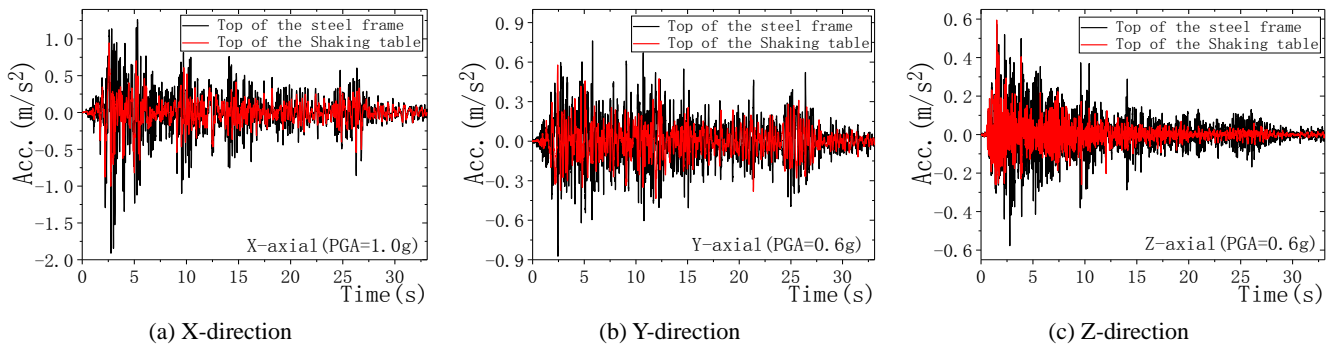


Fig. 13 Acceleration time history between the steel frame and the shaking table

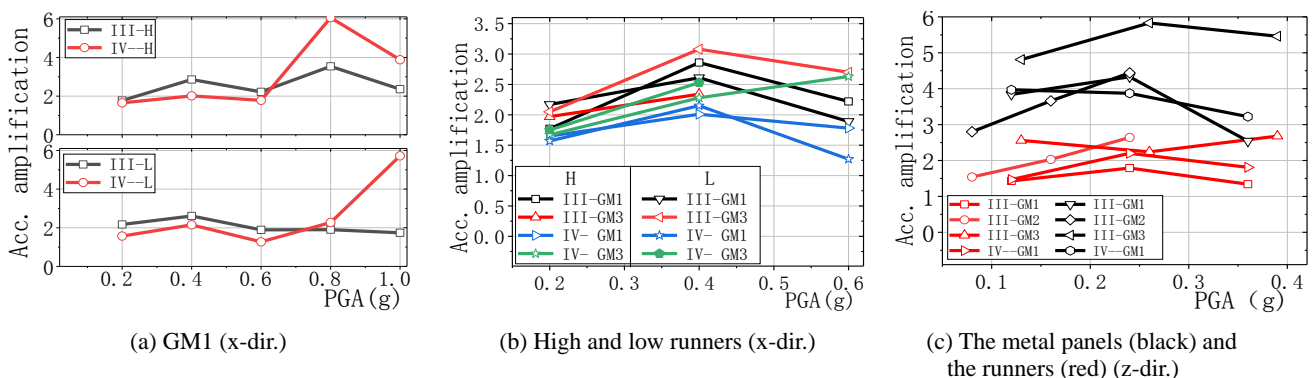


Fig. 14 Acceleration amplification of BMC components (H: high runners; L: low runners)

acceleration time history curve at the top of the steel frame is significantly enlarged compared with the peak of the acceleration time history curve of the shaking table. When $PGA \leq 1.2$ g, as the shaking table input intensity increased, the acceleration amplification factors at the top of the steel frame were mainly distributed in between 1.5~3. What's more, the slope of each line about the acceleration amplification is basically close to 1 (see Figs. 12(a)-(c)). Therefore, it can be considered that the steel frame could transmit seismic motion to the BMC system well. On the other hand, in the y-direction, the acceleration amplification of GM3 was apparently larger than that of GM1 and GM2 (see Fig. 12(b)), that is, the acceleration amplification of artificial wave was significantly higher than that of natural wave.

A key aspect of the ceiling response is the acceleration amplification of the ceiling components (runners) relative to the structural systems to which they are attached (top surface of steel beam) (Soroushian *et al.* 2016b). For $PGA \leq 0.6$ g, the acceleration amplification factors of steel runners in phase III were greater than that in phase IV, while it turned out to be the opposite result when $PGA \geq$

0.8 g (see Fig. 14(a)). It was discovered that the perimeter attachments of the cross runner would effectively increase the acceleration amplification factor under low earthquakes. And when $PGA \leq 0.6$ g, the acceleration amplification of the high runners and the low runners of BMC system was similar under earthquakes (see Fig. 14(b)), which is related to the good integrity of BMC system. The z-direction acceleration amplification of the metal panels was always larger than that of the runners (see Fig. 14(c)), which is due to the small out-of-plane stiffness of metal panel. This difference in the acceleration amplification caused the panels to fall and suggest that constraints of the metal panels may need to be increased. Finally, from the experiment data, the acceleration amplification factors of the steel runners were between 1.0 and 6.0, which were close to the results obtained by Soroushian *et al.* (2016b).

3.4 Displacement responses

The displacement of BMC mainly studied four parts: maximum relative displacement (MRD) between angle steel and steel beam in the x-direction (D1); MRD between metal

Table 5 Maximum relative displacement (MRD) (in millimeters)

Phase	PGA (g)	Ground motion	D1	X-dir.			D4	Phase	D1	X-dir.		
				D2	D3	D4				D2	D3	D4
Phase III	0.2	GM1	3.02	5.48	3.41	12.34	Phase IV	3.26	8.86	2.49	12.87	
		GM2	4.24	2.51	4.67	14.24		-	-	-	-	
		GM3	3.54	5.19	5.10	12.17		6.22	11.49	4.06	10.96	
	0.4	GM1	4.88	17.75	11.4	24.52		8.94	15.51	7.77	22.03	
		GM2	11.82	16.68	15.84	27.3		-	-	-	-	
		GM3	6.77	17.82	13.42	23.93		11.98	25.31	12.26	23.87	
	0.6	GM1	9.74	25.45	21.93	36.87		11.33	20.18	10.00	32.43	
		GM2	18.93	27.37	31.62	33.88		-	-	-	-	
		GM3	16.90	32.17	34.20	37.54		31.46	43.61	26.38	29.09	
	0.8	GM1	23.26	51.04	46.36	51.97		27.02	38.12	39.63	37.22	
		GM2	26.95	45.92	52.11	41.62		-	-	-	-	
		GM3	20.30	39.46	64.59	42.87		42.11	49.79	36.16	40.95	
1.0	GM1	28.40	50.29	63.03	66.64	47.75	73.04	50.81	69.60			
	GM3	35.28	85.67	78.81	44.02	-	-	-	-			

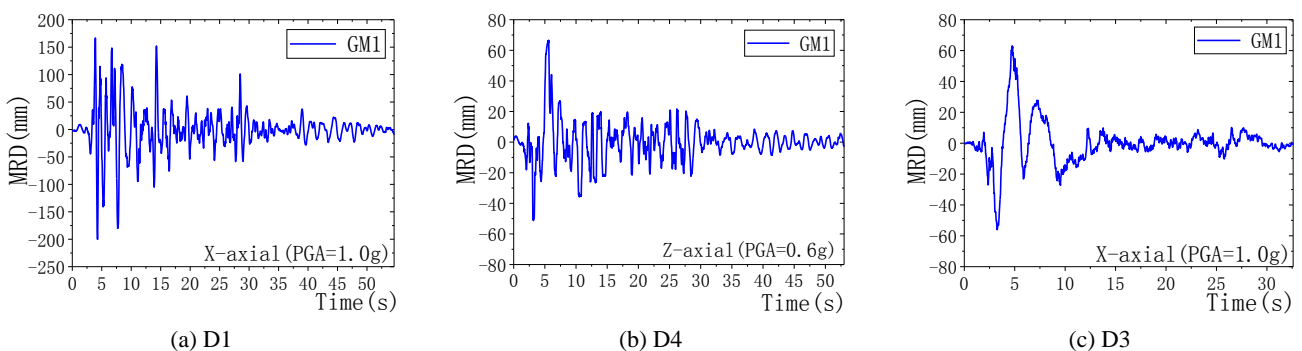


Fig. 15 Maximum relative displacement time history

panel and angle steel (D2); MRD between high metal panel and low metal panel (D3); and MRD between BMC and steel beam in the z-direction (D4). Table 5 shows MRD about the four parts. Fig. 15 shows the partial MRD time history. From Table 5, the following some points can be drawn:

- (1) The MRD between angle steel and steel beam which can be equivalent to the inter-story drift gradually increased as PGA augmented (see Fig. 16(a)). The maximum inter-story drift is one of the main parameters used in seismic design codes to guarantee a satisfactory seismic performance of structures (López-Barraza *et al.* 2016). In the x-direction and when PGA = 1.0 g, MRD between

angle steel and steel beam was 35.28 mm in Phase III, and 47.75 mm in Phase IV which translated into story drift angle of 1/10. According to the limit value elaso-plastic story drift rotation in Code for Seismic Design of Buildings GB50011-2010 (2016), though this story drift angle had far exceeded the limit value, BMC system was not suffered an overall failure.

- (2) MRD between high metal panel and low metal panel was always smaller than MRD between metal panel and angle steel, which is related to the integrity of BMC system. In the x-direction, D3 in Phase III was always greater than D3 in Phase IV (see Fig. 16(b)), indicating that removing the perimeter attachments of the cross runners would

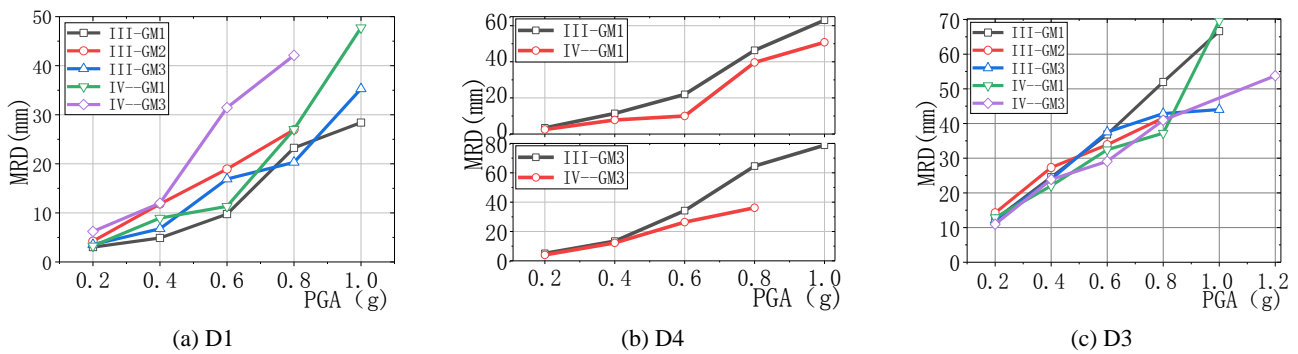


Fig. 16 Relative displacement

Table 6 Partial the maximum strain of measured points (10^{-6})

Case	S-1	S-5	S-6	S7-H	S7-V	S-8	S-10	S-11	
III-4 (0.2 g)	Max	216	114	438	176	26	202	108	32
	Min	-14	0	-16	-6	-6	-6	-2	-18
III-8 (0.4 g)	Max	524	272	246	376	42	280	104	82
	Min	-144	0	-68	-214	-44	-38	-50	-70
III-13 (0.6 g)	Max	584	186	140	594	40	376	186	188
	Min	-246	0	-66	-690	-292	-174	-86	-88
III-18 (0.8 g)	Max	760	156	466	622	366	294	154	220
	Min	-740	-36	-40	-1006	-38	-172	-116	-98
III-22 (1.0 g)	Max	982	244	598	-	-	310	244	292
	Min	-320	0	-108	-	-	-268	-54	-34
IV-3 (0.2 g)	Max	228	52	52	284	146	158	76	40
	Min	-210	-8	-114	-292	-76	-42	-12	-20
IV-5 (0.4 g)	Max	522	78	254	462	370	240	132	148
	Min	-296	-8	-166	-610	-116	-72	-14	-6
IV-8 (0.6 g)	Max	618	104	332	468	488	292	156	140
	Min	-560	-2	-246	-884	-86	-116	-50	-18
IV-11 (0.8 g)	Max	500	144	314	-	-	366	164	208
	Min	-828	-4	-192	-	-	-284	-138	-100
IV-14 (1.2 g)	Max	712	274	668	-	-	368	304	332
	Min	-1230	-6	-118	-	-	-144	-228	-142

*Note: 1) Pull positive, negative pressure about strain;

2) S7-H represents the horizontal of the z-profile camp. S7-V represents vertical directions of the z-profile camp

Table 7 Damage state of BMC

Limit state	MRD in the x-dir. (mm)	PGA(g)	Damage phenomena
Basically intact	$D3 \leq 31.62$	≤ 0.6	A sound, panel slipped
Slight	$31.62 \leq D3 \leq 63.03$	$0.6 \leq \text{PGA} \leq 0.8$	Nut loosen, a noise, panel derailed
Moderate	$63.03 \leq D3$	$0.8 \leq$	A loud collision sound, panel fell

reduce MRD between the components of BMC system. And MRD between BMC components under GM3 was larger than that of under GM1 and GM2. While in the z-direction, D4 was close under earthquakes, and it gradually increased with PGA augmented (see Fig. 16(c)).

- (3) Combined with the damage phenomena, several points were found under phase III and GM3. When D3 reached 13.42 mm in the x-direction, BMC system emitted a sound and the metal panels slightly slipped. When D3 reached 34.20 mm, BMC system emitted a noise and the metal panels derailed. When D3 reached 64.59 mm, BMC system emitted a loud collision sound and the metal panels fell.

3.5 Strain responses

In the discussion above, we can find that BMC system had the strongest seismic response under the action of GM3. Therefore, only the strains under GM3 were selected for analysis. Table 6 summarizes partial maximum strains of measured points which were useful. From the tests, the strains in phase III and phase IV were similar, that is, releasing the perimeter attachments of the cross runner had little effect on the strain variation of BMC system. By calculating the maximum strains, the maximum stress at the junction between the runner and the angle steel, the hanger rods, the Z-profile camp and the upper flange of the runners were, respectively, 246, 137.6, 207, 77.5 Mpa, which were all smaller than the corresponding yield strength (640, 235, 235, 235 Mpa).

3.6 Limit states analyses

According to the definition method of the suspended ceiling limit state by HAZUS-MH MR3 (FEMA 2003), the damage state of BMC was defined at Table 7. Limit state 1 was BMC emitted a sound and the metal panels slightly slipped, at this time, $D3 \leq 15.84$ mm in the x-direction ($\text{PGA} \leq 0.6$ g). Limit state 2 was BMC emitted a noise, nut loosened and the metal panels derailed, at this time, $D3 \leq 63.03$ mm in the x-direction ($0.6 \text{ g} \leq \text{PGA} \leq 0.8$ g). Limit state 3 was BMC emitted a loud collision sound and the metal panels fell, at this time, $63.03 \text{ mm} \leq D3$ in the x-direction ($0.8 \text{ g} \leq \text{PGA}$).

4. Conclusions

In this study, BMC was designed, manufactured and installed and then its seismic performance was evaluated by

shaking table tests. According to the test series, the following main conclusions could be drawn:

- For $\text{PGA} \leq 0.4$ g, there was basically no damage to the whole backdrop metal ceiling. For $0.6 \text{ g} \leq \text{PGA} \leq 1.2$ g, derailment or fall of a few metal panels, slippage of cross runners and loose of nuts occurred in the tests. But BMC as a whole remained intact in the experiments. After simple maintenance, BMC system could be restored to pre-earthquake state. The above shows that the design of BMC in this paper is reasonable and well-constructed.
- From the analysis of the damage phenomena, acceleration amplification and maximum relative displacement, the designed BMC had good integrity. In the experiments, the stress of components of BMC was smaller than the yield strength, and BMC did not cause serious damage, indicating that BMC system had reliable seismic performance throughout the test. Therefore, after adding the structural measures proposed in this paper, BMC can better provide theoretical basis and technical guidance for the seismic design of this type of ceiling system in engineering projects, especially in the main control area of nuclear power plants.
- For $\text{PGA} < 0.8$ g, MRD between high metal panel and low metal panel and the acceleration amplification of BMC system in phase IV were smaller than that in phase III, and the damage of BMC system in phase IV was less than that in phase III. That is because the ceiling components (panel and steel runner) were slipped after removing the perimeter attachments of the cross runners, giving BMC a certain cushioning effect. And the results show that the seismic performance of BMC system can be improved by removing the perimeter attachments of the cross runners.
- The response of BMC is hybrid-sensitive for acceleration and displacement. And we can conclude that falling of the metal panels in the experiment were caused by the acceleration increasing to a certain value ($\text{PGA} \geq 0.8$ g) and the maximum relative displacement between the high and low metal panels exceeding the limit (63.03 mm in the x-dir.).
- Considering the higher rigidity and frequency of the steel frame, the test results of BMC system are mainly applicable for limited cases in buildings whose main bearing structure has dynamic characteristics close to the dynamic characteristics of the steel frame used in this research.

Acknowledgments

The authors are very grateful to the laboratory teachers who worked overtime to help with the experiments. Special thanks are due to Qinghai Building and Materials Research Co., Ltd and The Key Lab of Plateau Building and Eco-community in Qinghai, China. They provided partial support and this support is gratefully acknowledged.

References

- Badillo-Almaraz, H. (2004), "Seismic qualification and fragility testing of suspended ceiling systems", *Proceedings of the 13th World Conference on Earthquake Engineering*, Vancouver, BC, Canada, August.
- Badillo-Almaraz, H., Whittaker, A.S., Reinhorn, A.M. and Cimellaro, G.P. (2006), "Seismic fragility of suspended ceiling systems", Report No. MCEER-06-0001; Department of Civil, Structural and Environmental Engineering, State University of New York, Buffalo, NY, USA.
- Bai, J.C. and Jin, J.P. (2007), "Discussion on seismic wave selection for time history analysis", *Shanxi Architecture*, **33**(3), 62-63. <https://doi.org/10.3969/j.issn.1009-6825.2007.03.038>
- Baloević, G., Radnić, J., Grgić, N. and Matešan, D. (2016), "The application of a reinforced plaster mortar for seismic strengthening of masonry structures", *Compos. Part B, Eng.*, **93**, 190-202. <https://doi.org/10.1016/j.compositesb.2016.03.007>
- Baloevic, G., Radnic, J., Grgic, N. and Matesan, D. (2017), "Shake-table study of plaster effects on the behavior of masonry-infilled steel frames", *Steel Compos. Struct., Int. J.*, **23**(2), 195-204. <https://doi.org/10.12989/scs.2017.23.2.195>
- Banović, I., Radnić, J., Grgić, N. and Matešan, D. (2018), "The use of limestone sand for the seismic base isolation of structures", *Adv. Civil Eng.* <https://doi.org/10.1155/2018/9734283>
- Echevarria, A.A., Zaghi, A.E., Soroushian, S. and Maragakis, M. (2012), "Seismic fragility of suspended ceiling systems", *Proceedings of the 15th World Conference on Earthquake Engineering*, Lisboa, Portugal, September.
- FEMA (2003), Multi-hazard loss estimation methodology, earthquake model, HAZUS-MH MR3; Washington, DC, USA.
- GB50011-2010 (2016), Code for seismic design of buildings, China Architecture & Building Press; Beijing, China.
- Gilani, A.S.J., Reinhorn, A.M., Glasgow, B., Lavan, O. and Miyamoto, H.K. (2010), "Earthquake simulator testing and seismic evaluation of suspended ceilings", *J. Architect. Eng.*, **16**(2), 63-73. [https://doi.org/10.1061/\(ASCE\)1076-0431\(2010\)16:2\(63\)](https://doi.org/10.1061/(ASCE)1076-0431(2010)16:2(63))
- Han, Q.H., Zhang, P. and Lu, Y. (2014), "Dynamic performance of non-structural components in large span buildings based on transfer function", *China Civil Eng. J.*, **47**(S2), 79-84. <https://doi.org/10.15951/j.tmgcvb.2014.s2.013>
- López-Barraza, A., Ruiz, S.E., Reyes-Salazar, A. and Bojórquez, E. (2016), "Demands and distribution of hysteretic energy in moment resistant self-centering steel frames", *Steel Compos. Struct., Int. J.*, **20**(5), 1155-1171. <https://dx.doi.org/10.12989/scs.2016.20.5.1155>
- Lu, Y., Mosqueda, G., Han, Q.H. and Zhao, Y.F. (2018), "Shaking table tests examining seismic response of suspended ceilings attached to large-span spatial structures", *J. Struct. Eng.*, **144**(9), 04018152. [https://doi.org/10.1061/\(ASCE\)ST.1943-541X.0002140](https://doi.org/10.1061/(ASCE)ST.1943-541X.0002140)
- Magliulo, G., Pentangelo, V., Maddaloni, G., Capozzi, V., Petrone, G., Lopez, P., Talamonti, R. and Manfredi, G. (2012), "Shake table tests for seismic assessment of suspended continuous ceilings", *Bull. Earthq. Eng.*, **10**(6), 1819-1832. <https://doi.org/10.1007/s10518-012-9383-6>
- Ozcelik, O., Misir, I.S., Saridogan, S. and Saridogan, S. (2016), "Performance evaluation of suspended ceiling systems using shake table test", *Struct. Eng. Mech., Int. J.*, **58**(1), 121-142. <https://doi.org/10.12989/sem.2016.58.1.121>
- Radnić, J., Grgić, N., Matešan, D. and Baloević, G. (2015), "Shake table testing of reinforced concrete columns with different layout size of foundation", *Materialwissenschaft und Werkstofftechnik*, **46**(4-5), 348-367. <https://doi.org/10.1002/mawe.201500410>
- Sato, E., Furukawa, S., Kakehi, A. and Nakashima, M. (2011), "Full-scale shaking table test for examination of safety and functionality of base-isolated medical facilities", *Earthq. Eng. Struct. Dyn.*, **40**(13), 1435-1453. <https://doi.org/10.1002/eqe.1097>
- Shen, J.M. (2015), *Aseismic Engineering*, (2th Edition), China Architecture & Building Press, Beijing, China.
- Soroushian, S., Maragakis, M. and Jenkins, C. (2016a), "Capacity evaluation of suspended ceiling-perimeter attachments", *J. Struct. Eng.*, **142**(2), 04015124. [https://doi.org/10.1061/\(ASCE\)ST.1943-541X.0001355](https://doi.org/10.1061/(ASCE)ST.1943-541X.0001355)
- Soroushian, S., Rahmanishamsi, E., Ryu K.P., Maragakis, M. and Reinhorn, A.M. (2016b), "Experimental fragility analysis of suspension ceiling systems", *Earthq. Spectra*, **32**(2), 881-908. <https://doi.org/10.1193/071514EQS109M>
- Wang, D.Z., Dai, J.W., Qu Z. and Ning, X.Q. (2016), "Shake table tests of suspended ceilings to simulate the observed damage in them 7.0 lushan earthquake, china", *Earthq. Eng. Eng. Vib.*, **15**(2), 239-249. <https://doi.org/10.1007/s11803-016-0319-z>
- Watakabe, M., Iuui, S., Ishioka, T., Iizuka, S., Takai, S. and Kanagawa, M. (2012), "A study on the behavior of seismically engineered ceiling systems of large open structures subjected to earthquake excitation", *Proceedings of the 15th World Conference on Earthquake Engineering*, Lisboa, Portugal, September.
- Yao, G.C. (2000), "Seismic performance of direct hung suspended ceiling systems", *J. Architect. Eng.*, **6**(1), 6-11. [https://doi.org/10.1061/\(ASCE\)1076-0431\(2000\)6:1\(6\)](https://doi.org/10.1061/(ASCE)1076-0431(2000)6:1(6))
- Zhang, J. (2002), "Using MATLAB to deal with data of the shaking table test", *Industrial Building*, **32**(2), 28-31. <https://doi.org/10.3321/j.issn:1000-8993.2002.02.009>
- Zhang, W., Chen, Z.H., Xiong, Q.Q. and Zhou, T. (2018), "Experimental seismic behaviour of L-CFST column to H-beam connections", *Steel Compos. Struct., Int. J.*, **26**(6), 793-808. <https://doi.org/10.12989/scs.2018.26.6.793>

CC

Appendix I. Shaking Table Specifications

Parameter	Description
Degree of freedom	6
Table size	4.1×4.1 m
Payload	20t (full payload); 30 t (payload reduction)
Frequency bandwidth	0.1~50 Hz
Stroke	x: ±150 mm; y: ±250 mm; z: ±100 mm
Peak acceleration (full payload)	x: ±1.2 g; y and z: ±1.0 g

Appendix II. Steel sections of test frame

Steel element	Section (mm)	Yield strength (MPa)	Remarks
Steel column	φ219×12		
Main beam	I300a	235	All steel materials are Q235b, and the total mass of the steel frame is 3.3t.
Secondary beam	I200b		

Appendix III. Key properties of ceiling components

Ceiling component	Type and specification	Total mass (kg)	Material	Yield strength f_y (MPa)	Elastic modulus (MPa)
Hanger rod (500 mm)	M8	4.864			
Hanger rod (250 mm)	M8	1.824			
hanger clip	100×20×2	2.968	Q235	235	206000
Main runner	C50×15×1.2	29.541			
Cross runner	Z55×25×10×1.5	54.880			
Z-profile camp	60×70×1	5.070			
L-shaped metal panel	600×600×350×2	102.192			
Metal panel	600×600×2	79.800	Aluminum alloy	260	206000
Headlight	1200×600	13.150			
Other light	600×600	6.750			
Nut	M6	-	8.8 grade steel	640	200000